

Article

Finite-Time Adaptive Synchronization and Fixed-Time Synchronization of Fractional-Order Memristive Cellular Neural Networks with Time-Varying Delays

Yihong Liu ¹  and Yeguo Sun ^{2,*} ¹ School of Computer Science, Huainan Normal University, Huainan 232038, China; liuyh@hnnu.edu.cn² School of Finance and Mathematics, Huainan Normal University, Huainan 232038, China

* Correspondence: yeguosun@126.com

Abstract: Asymptotic synchronization requires continuous external control of the system, which is unrealistic considering the cost of control. Adaptive control methods have strong robustness to uncertainties such as disturbances and unknowns. On the other hand, for finite-time synchronization, if the initial value of the system is unknown, the synchronization time of the finite-time synchronization cannot be estimated. This paper explores the finite-time adaptive synchronization (FTAS) and fixed-time synchronization (FDTS) of fractional-order memristive cellular neural networks (FMCNNs) with time-varying delays (TVD). Utilizing the properties and principles of fractional order, we introduce a novel lemma. Based on this lemma and various analysis techniques, we establish new criteria to guarantee FTAS and FDTS of FMCNNs with TVD through the implementation of a delay-dependent feedback controller and fractional-order adaptive controller. Additionally, we estimate the upper bound of the synchronization setting time. Finally, numerical simulations are conducted to confirm the validity of the finite-time and fixed-time stability theorems.

Keywords: finite-time adaptive synchronization; fixed-time synchronization; fractional-order memristive cellular neural networks; time-varying delays

MSC: 68T07



Citation: Liu, Y.; Sun, Y. Finite-Time Adaptive Synchronization and Fixed-Time Synchronization of Fractional-Order Memristive Cellular Neural Networks with Time-Varying Delays. *Mathematics* **2024**, *12*, 1108. <https://doi.org/10.3390/math12071108>

Academic Editor: Jonathan Blackledge

Received: 24 February 2024

Revised: 23 March 2024

Accepted: 2 April 2024

Published: 7 April 2024



Copyright: © 2024 by the authors. Licensee MDPI, Basel, Switzerland. This article is an open access article distributed under the terms and conditions of the Creative Commons Attribution (CC BY) license (<https://creativecommons.org/licenses/by/4.0/>).

1. Introduction

Memristive neural networks (MNNs) have garnered significant research interest due to their applications in various fields, including image processing, combinatorial optimization, and artificial intelligence (see [1–3]). Differing from traditional neural networks, MNNs are an enhanced version where conventional resistors are substituted with memristors. It is well established that a memristor is a type of resistor possessing memory capabilities, and it can memorize the route through an electric charge [4]. This category of dynamical systems is characterized by state-dependent switched discontinuous systems, which can readily result in complex behaviors and switching uncertainties. Therefore, the dynamical analysis of MNNs is a crucial area of study in both theoretical and applied contexts (see [5,6]). It is widely acknowledged that fractional-order neural networks possess numerous advantages over their integer-order counterparts. Subsequently, fractional-order neural networks have garnered significant interest from researchers, leading to a wealth of insightful findings regarding their dynamical behaviors (see [7–9]).

Cellular neural networks (CNNs) are large-scale nonlinear analog circuits that process signals in real time. CNNs are composed of regularly spaced cells. However, as the number of cells in the CNNs increases, the circuit structure of the CNNs becomes complex, which can make it inconvenient to update the weight templates. If memristors are used to implement synaptic connections within the CNNs, it can reduce area consumption and power consumption, and the conditions for updating weights become simpler. Due to the

inherent memory characteristics of memristors, the information processing capabilities of the memristor cellular neural networks (MCNNs) are enhanced (see [10,11]).

Fractional calculus is an extension of integer calculus. It is characterized by taking into account the current state and all previous states, exhibiting a memory property. It is widely used as a mathematical tool in fields such as pattern recognition, information processing, robot control, physics, statistics, and more. In practical applications, the fractional order is often used to establish neural network models (see [12–16]).

In the practical application of neural networks, the processing and transmission of signals between neurons are limited by the switching speed of amplifiers. A time delay is inevitable, which affects the stability of the neural network and leads to divergence, instability, and oscillation of the network system. Delays include constant delays and time-varying delays, which are considered more effective than constant delays in establishing neural network systems. Neural networks with TVD are more capable of solving complex practical problems (see [17–20]).

Synchronization refers to the dynamic behavior wherein a system, through processes of driving and responding, achieves a state of congruence after a specified duration. Synchronous technology, with its potential applications in medicine, information science, optimization computing, and automatic control, has garnered significant attention in recent years. It assumes multiple forms, for instance, asymptotical synchronization [21,22], exponential synchronization [23,24], robust synchronization [25], finite-time synchronization [26–31], fixed-time synchronization [32–35], and so on. In practical applications, due to objective constraints, we usually hope to achieve synchronization of the neural network drive response within a limited time. Furthermore, the finite-time and fixed-time control techniques have also demonstrated superior interference suppression performance and robustness.

In recent years, there have been significant advancements in the study of finite-time synchronization (FTS) for memristive neural network systems. For instance, see [36–43]. Li et al. [36] investigated FTS for a class of drive-response FMNNs with discontinuous activation functions. Li et al. [37] explored the FTS and FDTS of coupled MNNs with discontinuous feedback functions. Li et al. [38] discussed the FTAS and FTS of MNNs with discontinuous activation functions and mixed time-varying delays. Zhang et al. [39] studied the FTS of fractional-order complex-valued MNNs with delay. Guo et al. [40] proposed FTS of drive-response inertial MNNs with time delay. Wei et al. [41], utilizing interval-matrix-based methods, investigated the FTS/FTDS of delayed inertial MNNs. Gong et al. [42] focused on the FTS problem of fuzzy MNNs with time delay. Zhao et al. [43] investigated FTS for a class of FOMFNNs with leakage and transmission delays.

However, independent of initial conditions, finite-time synchronous control methods cannot ensure the system's convergence within a predetermined time frame. When the initial state information is unknown, the application of these methods becomes restricted by the lack of initial conditions. Researchers have initiated investigations into the issue of the FDTS control problem and have attained preliminary findings. For instance, Arslan et al. [44] investigated the controller design problem for FTDS of fractional-order memristive complex-valued BAM neural networks. Wang et al. [45], utilizing a fractional-order sliding-mode control method, investigated the FDTS control problem of MNNs. Xiao et al. [46] discussed the FDTS control problem of memristive neural networks with delay. Wang et al. [47], utilizing impulsive effects via the novel fixed-time stability theorem, investigated the FDTS control problem of memristive neural networks with delay. Although MNNs have achieved good results in finite-time synchronization and fixed-time synchronization, there is still a lack of research on finite-time and fixed-time synchronization of FMNNs, especially for FMNNs with mixed time-varying delays, which has driven our investigation.

As far as the author knows, the FTAS and FDTS of FMCNNs with TVD have not been fully studied. The main contributions of this article are summarized as follows:

- For the first time, the FTAS and FDTS of FMCNNs with TVD are studied. In practical applications, FTAS and FDTS are more general and practical than finite-time synchronization and asymptotic synchronization;
- By constructing a nonlinear feedback controller and choosing a simple Lyapunov function, some sufficient conditions which are easy to verify are obtained to ensure the finite-time and fixed-time stability of FMCNNs and the FTAS and FDTS of the drive-response FMCNNs systems;
- The theoretical results obtained are more general and can improve or supplement previous results effectively. Moreover, the existing FMCNNs model with no fuzzy logic, no time-varying delay, and no memristor can all be regarded as the special case of our model;
- The settling time in this paper is easy to estimate. In addition, compared with the classical results, the estimation bound of the settling time given in our paper is more accurate and effective. Numerical examples are given to demonstrate the effectiveness of the proposed approaches.

This study examines the FTAS and FTS of FMCNNs with TVD. By harnessing the properties and principles inherent to fractional-order systems, a novel lemma is introduced. Building upon this lemma and employing various analytical techniques, new criteria are formulated to ensure FTAS and FTS of FMCNNs with TVD. This is achieved through the application of a feedback controller and a fractional-order adaptive controller. Furthermore, an estimation of the upper bound for the synchronization setting time is provided.

The rest of this paper is organized as follows. Several preliminaries will be provided in Section 2, and theoretical results will be derived in Sections 3 and 4. In Section 5, numerical simulations will be given to verify the obtained theoretical results. A conclusion will be presented in Section 6.

Notations: In this paper, the symbols can be elucidated as follows: R represents the set of real numbers; N represents the set of natural numbers; Z^+ represents a set of positive integers; R^m denotes a m -dimensional vector space; $C^m[a, b]$ is used to denote the set of continuous functions with an n -th-order derivative on the interval $[a, b]$.

2. Preliminaries and Model Description

In this article, the system model is defined by the Caputo fractional order. Some basic definitions, lemmas, and assumptions about fractional calculus are introduced.

Definition 1 ([48]). *The Caputo fractional integral of the function $\chi(t)$ is defined as follows:*

$${}^C_{t_0}D^{-\omega}\chi(t) = \frac{1}{\Gamma(\omega)} \int_{t_0}^t (t-v)^{\omega-1}\chi(v)dv, \tag{1}$$

where $\omega > 0, t > t_0, \Gamma(\cdot)$ is the gamma function.

Definition 2 ([48]). *The Caputo fractional derivative of the function $\chi(t)$ is defined as follows:*

$${}^C_{t_0}D^\omega\chi(t) = \frac{1}{\Gamma(n-\omega)} \int_{t_0}^t (t-v)^{n-\omega-1}\chi^{(n)}(v)dv, \tag{2}$$

where $t > t_0, \omega \in (n-1, n], n \in Z^+$. If $\omega \in (0, 1]$. Then,

$${}^C_{t_0}D^\omega\chi(t) = \frac{1}{\Gamma(1-\omega)} \int_{t_0}^t \frac{\chi'(v)}{(t-v)^\omega}dv.$$

Lemma 1 ([49]). *If $\omega \geq \gamma \geq 0$, the following equation always holds:*

$${}^C_{t_0}D^\omega D^{-\gamma}\chi(t) = {}^C_{t_0}D^{\omega-\gamma}\chi(t) \tag{3}$$

When $\omega = \gamma$,

$${}^C_{t_0}D^\omega D^{-\gamma}\chi(t) = \chi(t)$$

Lemma 2 ([49]). Denote $m = [\omega] + 1$ for $\omega \notin N$ or $n = \omega$ for $\omega \in N$. If $\chi(t) \in C^m[a, b]$, then Equation(4) holds.

$${}^C_{t_0}D^{-\omega}D^\omega\chi(t) = \chi(t) - \sum_{k=0}^{n-1} \frac{\chi^{(k)}(\omega)}{k!} (\chi(t) - \omega)^k \tag{4}$$

Obviously, if $0 < \omega < 1$ and $\chi(t) \in C^1[a, b]$, then

$${}^C_{t_0}D^{-\omega}D^\omega\chi(t) = \chi(t) - \chi(\omega)$$

Lemma 3 ([50]). If $\chi(t) \in C^1[t_0, \infty]$, $0 < \omega \leq 1$, then Equation (5) holds.

$${}^C_{t_0}D^\omega|\chi(t)| \leq \text{sign}(\chi(t)){}^C_{t_0}D^\omega\chi(t) \tag{5}$$

Lemma 4 ([51]). For $\forall \beta \in R$. If $\chi(t) \in C^1[t_0, \infty]$, $0 < \omega \leq 1$, Equation (6) holds.

$${}^C_{t_0}D^\omega(\chi(t) - \beta)^2 \leq 2(\chi(t) - \beta){}^C_{t_0}D^\omega\chi(t) \tag{6}$$

Lemma 5 ([52]). If $\alpha_1, \alpha_2, \dots, \alpha_M \geq 0, 0 < \nu \leq 1, \mu > 1$, then Equation (7) holds.

$$\sum_{k=1}^M \alpha_k^\mu \geq M^{1-\mu} \left(\sum_{k=1}^M \alpha_k \right)^\mu, \sum_{k=1}^M \alpha_k^\nu \geq \left(\sum_{k=1}^M \alpha_k \right)^\nu \tag{7}$$

Lemma 6 ([9]). If there exists a positive-definite function $V(\Delta(t)) : R^m \rightarrow R$ which satisfies the inequality

$${}^C_{t_0}D^\omega V(\Delta(t)) \leq -\gamma \tag{8}$$

where $\gamma > 0$ is a constant, then the origin is finite-time stable for all $t \geq T_{max}$. T_{max} is given by:

$$T_{max} = t_0 + \left(\frac{\Gamma(1 + \omega)V(\Delta(t_0))}{\gamma} \right)^{\frac{1}{\omega}} \tag{9}$$

Lemma 7 ([35]). If there exists a positive-definite function $V(\Delta(t)) : R^m \rightarrow R$ which satisfies the inequality

$$\dot{V}(\Delta(t)) \leq - \left(aV^\delta(\Delta(t)) + b \right)^k, \Delta(t) \in R^m \setminus 0 \tag{10}$$

where $a, b, \delta, k > 0$ are constants and $\delta k > 1$, then the origin is fixed-time stable for all $t \geq T_{max}$. T_{max} is given by:

$$T_{max} = \frac{1}{b^k} \left(\frac{b}{a} \right)^{\frac{1}{\delta}} \left(1 + \frac{1}{\delta k - 1} \right) \tag{11}$$

Next, we consider an FMCNN with mixed time-varying delays as follows:

$$\begin{cases} {}^C_{t_0}D^\omega p_i(t) = -\alpha_i p_i(t) + \sum_{r=1}^M \phi_{ir}(p_i(t))f_r(p_r(t)) \\ \quad + \sum_{r=1}^M \psi_{ir}(p_i(t))f_r(p_r(t - \tau(t))) + \varepsilon \sum_{r=1}^M d_{ir}g_r(q_r(t)) + I_i \\ p_i(v) = \zeta_i(v), v \in [-\tau, t_0], i = 1, \dots, M, \end{cases} \tag{12}$$

where $p_i(t)$ represents the corresponding state. $\alpha_i > 0$ denotes the self-feedback connection weight. ε represents the interaction weight. d_{ir} represents the interaction structure. $f_r(\cdot)$ is the activation function. $g_r(\cdot)$ is an interaction function. $\tau(t)$ denotes time-varying delay,

and $\tau(t) \in [0, \tau]$, $\phi_{ir}(p_i(t))$, and $\psi_{ir}(p_i(t))$ represent the memristive connection weights. I_i represents the bias value, and

$$\phi_{ir}(p_i(t)) = \frac{F_{ir}}{C_i} \times s_{ir}, \psi_{ir}(p_i(t)) = \frac{F_{ir}^*}{C_i} \times s_{ir}, s_{ir} = \begin{cases} 1, i \neq r \\ -1, i = r \end{cases}$$

where F_{ir}, F_{ir}^* represent the memory resistance value of the memristors E_{ir}, E_{ir}^* , respectively. Here, E_{ir}, E_{ir}^* indicate the memristor between $f_r(p_r(t))$ and $p_i(t)$ and $f_r(p_r(t - \tau(t)))$ and $p_i(t)$, respectively. Based on the characteristics of the memristor, we set the following values for the memristor’s jumps:

$$\phi_{ir}(p_i(t)) = \begin{cases} \phi'_{ir}, |p_i(t)| \leq \Gamma_i \\ \phi''_{ir}, |p_i(t)| > \Gamma_i \end{cases}$$

$$\psi_{ir}(p_i(t)) = \begin{cases} \psi'_{ir}, |p_i(t)| \leq \Gamma_i \\ \psi''_{ir}, |p_i(t)| > \Gamma_i \end{cases}$$

where $\Gamma_i > 0$ is the switching jump value of the memristor, and $\phi'_{ir}, \phi''_{ir}, \psi'_{ir}, \psi''_{ir}$ are known constants. $\zeta_i(v)$ represents the initial values of system (12).

The response system is described as follows:

$$\begin{cases} {}^C_{t_0} D^\omega q_i(t) = -\alpha_i q_i(t) + \sum_{r=1}^M \phi_{ir}(q_i(t)) f_r(q_r(t)) \\ \quad + \sum_{r=1}^M \psi_{ir}(q_i(t)) f_r(q_r(t - \tau(t))) + \varepsilon \sum_{r=1}^M \hat{d}_{ir} g_r(p_r(t)) + I_i + u_i(t) \\ q_i(v) = \zeta_i(v), v \in [-\tau, t_0], i = 1, \dots, M, \end{cases} \tag{13}$$

where \hat{d} represents the interaction structure. $u_i(t)$ is the control input, and

$$\phi_{ir}(q_i(t)) = \begin{cases} \phi'_{ir}, |q_i(t)| \leq \Gamma_i \\ \phi''_{ir}, |q_i(t)| > \Gamma_i \end{cases}$$

$$\psi_{ir}(q_i(t)) = \begin{cases} \psi'_{ir}, |q_i(t)| \leq \Gamma_i \\ \psi''_{ir}, |q_i(t)| > \Gamma_i \end{cases}$$

where $\zeta_i(v)$ represents the initial values of system (13).

Let $\Delta_i(t) = q_i(t) - p_i(t)$ be the synchronization error. Then, the error system is described as follows:

$$\begin{cases} {}^C_{t_0} D^\omega \Delta_i(t) = -\alpha_i \Delta_i(t) + G_i(t) + u_i(t) \\ \Delta_i(v) = \zeta_i(v) - \zeta_i(v), v \in [-\tau, t_0], i = 1, 2, \dots, M. \end{cases} \tag{14}$$

where

$$G_i(t) = \sum_{r=1}^M \phi_{ir}(q_i(t)) f_r(q_r(t)) - \sum_{r=1}^M \phi_{ir}(p_i(t)) f_r(p_r(t))$$

$$+ \sum_{r=1}^M \psi_{ir}(q_i(t)) f_r(q_r(t - \tau(t))) - \sum_{r=1}^M \psi_{ir}(p_i(t)) f_r(p_r(t - \tau(t)))$$

Assumption 1. For $\forall \mu, v \in R$, there exists constants $Q_r, Q'_r > 0$ such that

$$|f_r(\mu) - f_r(v)| \leq Q_r |\mu - v|, |g_r(\mu) - g_r(v)| \leq Q'_r |\mu - v|, r = 1, 2, \dots, M.$$

Assumption 2. There exists constants $S_r, S'_r > 0$, such that $|f_r(\cdot)| \leq S_r, |g_r(\cdot)| \leq S'_r, r = 1, 2, \dots, M$.

Lemma 8. If Assumptions 1 and 2 satisfy, then Equation (15) holds.

$$|G_i(t)| \leq \sum_{r=1}^M \left[(\tilde{\phi}_{ir} Q_r + \varepsilon \tilde{d}_{ir} Q'_r) |\Delta_r(t)| + |\phi'_{ir} - \phi''_{ir}| S_r + \tilde{\psi}_{ir} Q_r |\Delta_r(t - \tau(t))| + |\psi'_{ir} - \psi''_{ir}| S_r + \varepsilon |\hat{d}_{ir} - d_{ir}| S'_r \right] \tag{15}$$

where $\tilde{\phi}_{ir} = \max\{|\phi'_{ir}|, |\phi''_{ir}|\}, \tilde{\psi}_{ir} = \max\{|\psi'_{ir}|, |\psi''_{ir}|\}, \tilde{d}_{ir} = \max\{|\hat{d}_{ir}|, |d_{ir}|\}, i, r = 1, 2, \dots, M$.

Proof.

$$\begin{aligned} G_i(t) &= \sum_{r=1}^M \phi_{ir}(q_i(t)) f_r(q_r(t)) - \sum_{r=1}^M \phi_{ir}(q_i(t)) f_r(p_r(t)) \\ &\quad + \sum_{r=1}^M \phi_{ir}(q_i(t)) f_r(p_r(t)) - \sum_{r=1}^M \phi_{ir}(p_i(t)) f_r(p_r(t)) \\ &\quad + \sum_{r=1}^M \psi_{ir}(q_i(t)) f_r(q_r(t - \tau(t))) - \sum_{r=1}^M \psi_{ir}(q_i(t)) f_r(p_r(t - \tau(t))) \\ &\quad + \sum_{r=1}^M \psi_{ir}(q_i(t)) f_r(p_r(t - \tau(t))) - \sum_{r=1}^M \psi_{ir}(p_i(t)) f_r(p_r(t - \tau(t))) \\ &\quad + \varepsilon \sum_{r=1}^M \hat{d}_{ir} g_r(p_r(t)) - \varepsilon \sum_{r=1}^M d_{ir} g_r(q_r(t)) \\ &= \sum_{r=1}^M \phi_{ir}(q_i(t)) [f_r(q_r(t)) - f_r(p_r(t))] + \sum_{r=1}^M [\phi_{ir}(q_i(t)) - \phi_{ir}(p_i(t))] f_r(p_r(t)) \\ &\quad + \sum_{r=1}^M \psi_{ir}(q_i(t)) [f_r(q_r(t - \tau(t))) - f_r(p_r(t - \tau(t)))] \\ &\quad + \sum_{r=1}^M [\psi_{ir}(q_i(t)) - \psi_{ir}(p_i(t))] f_r(p_r(t - \tau(t))) + \varepsilon \left[\sum_{r=1}^M \hat{d}_{ir} g_r(p_r(t)) - \sum_{r=1}^M d_{ir} g_r(q_r(t)) \right] \end{aligned}$$

due to

$$\begin{aligned} \sum_{r=1}^M \hat{d}_{ir} g_r(p_r(t)) - \sum_{r=1}^M d_{ir} g_r(q_r(t)) &= \sum_{r=1}^M \hat{d}_{ir} g_r(p_r(t)) - \sum_{r=1}^M d_{ir} g_r(p_r(t)) \\ &\quad + \sum_{r=1}^M d_{ir} g_r(p_r(t)) - \sum_{r=1}^M d_{ir} g_r(q_r(t)) \end{aligned}$$

or

$$\begin{aligned} \sum_{r=1}^M \hat{d}_{ir} g_r(p_r(t)) - \sum_{r=1}^M d_{ir} g_r(q_r(t)) &= \sum_{r=1}^M \hat{d}_{ir} g_r(p_r(t)) - \sum_{r=1}^M \hat{d}_{ir} g_r(q_r(t)) \\ &\quad + \sum_{r=1}^M \hat{d}_{ir} g_r(q_r(t)) - \sum_{r=1}^M d_{ir} g_r(q_r(t)) \end{aligned}$$

Based on Assumptions 1 and 2, we can obtain the following:

$$\begin{aligned}
 |G_i(t)| &\leq \sum_{r=1}^M \left[\tilde{\phi}_{ir} Q_r |\Delta_r(t)| + |\phi'_{ir} - \phi''_{ir}| S_r + \tilde{\psi}_{ir} Q_r |\Delta_r(t - \tau(t))| \right. \\
 &\quad \left. + |\psi'_{ir} - \psi''_{ir}| S_r + \varepsilon |\hat{d}_{ir} - d_{ir}| S'_r + \varepsilon \tilde{d}_{ir} Q'_r |\Delta_r(t)| \right] \\
 &= \sum_{r=1}^M \left[(\tilde{\phi}_{ir} Q_r + \varepsilon \tilde{d}_{ir} Q'_r) |\Delta_r(t)| + |\phi'_{ir} - \phi''_{ir}| S_r + \tilde{\psi}_{ir} Q_r |\Delta_r(t - \tau(t))| \right. \\
 &\quad \left. + |\psi'_{ir} - \psi''_{ir}| S_r + \varepsilon |\hat{d}_{ir} - d_{ir}| S'_r \right]
 \end{aligned}$$

This completes the proof. \square

3. Finite-Time Adaptive Synchronization Control

In this section, we discuss the finite-time synchronization of FMCNNs (12) and (13). To achieve the finite-time synchronization between (12) and (13), the controller is designed as:

$$u_i(t) = -\kappa_i \Delta_i(t) - \text{sign}(\Delta_i(t)) \sum_{r=1}^M \theta_{ir} |\Delta_r(t - \tau(t))| - \delta_i \text{sign}(\Delta_i(t)) \tag{16}$$

and

$$\begin{cases}
 u_i(t) = -\kappa_i(t) \Delta_i(t) - \text{sign}(\Delta_i(t)) \sum_{r=1}^M \theta_{ir}(t) |\Delta_r(t - \tau(t))| - \delta_i \text{sign}(\Delta_i(t)) \\
 {}^C_{t_0} D^\omega \kappa_i(t) = \lambda_i |\Delta_i(t)| - \frac{1}{2} (\kappa_i(t) - \hat{\kappa}_i) \\
 {}^C_{t_0} D^\omega \theta_{ir}(t) = \rho_i |\Delta_i(t - \tau(t))| - \frac{1}{2} (\theta_{ir}(t) - \hat{\theta}_{ir})
 \end{cases} \tag{17}$$

where $\kappa_i > 0, \delta_i > 0, \theta_{ir} > 0, \lambda_i > 0, \rho_i > 0, \hat{\kappa}_i, \hat{\theta}_{ir}$ are adaptive constants. $\kappa_i(t), \theta_{ir}(t)$ are the adaptive control gains. $\text{sign}(\cdot)$ is the symbolic function.

Remark 1. The feedback controller (16) and adaptive controller (17) are different. The controller (17) has fractional derivative behavior and can reduce control costs by using state information. In (16) and (17), the terms with time-varying delays are to remove the time delays, and the control gain δ_i can improve the fast response. When δ_i is greater, the system synchronization error will oscillate.

Theorem 1. If Assumptions 1 and 2 hold, and control gains $\kappa_i, \theta_{ir}, \delta_i$ satisfy $\kappa_i \geq -\alpha_i + \sum_{r=1}^M (\tilde{\phi}_{ri} Q_r + \varepsilon \tilde{d}_{ri} Q'_r), \theta_{ir} \geq \tilde{\psi}_{ir} Q_r, \delta_i > \sum_{r=1}^M (|\phi'_{ri} - \phi''_{ri}| S_r + |\psi'_{ri} - \psi''_{ri}| S_r + \varepsilon |\hat{d}_{ri} - d_{ri}| S'_r), i, r = 1, 2, \dots, M$, then FMCNNs (12) and (13) can realize finite-time synchronization under the feedback controller (16). Furthermore, the upper bound time for synchronization is calculated by (18).

$$T_{max} = t_0 + \left(\frac{\Gamma(1 + \omega) V(t_0)}{\sum_{i=1}^M \min_{1 \leq i \leq M} \{c_i\}} \right)^{\frac{1}{\omega}}. \tag{18}$$

Proof. Consider the Lyapunov function:

$$V(\Delta_i(t)) = \sum_{i=1}^M |\Delta_i(t)| \tag{19}$$

\square

Using Lemma 3, we calculate the fractional derivative of (18).

$$\begin{aligned}
 {}^C_{t_0}D^\omega V(\Delta(t)) &= \sum_{i=1}^M {}^C_{t_0}D^\omega |\Delta_i(t)| \leq \sum_{i=1}^M \text{sign}(\Delta_i(t)) {}^C_{t_0}D^\omega \Delta_i(t) \\
 &= \sum_{i=1}^M \text{sign}(\Delta_i(t)) \left[-\alpha \Delta_i(t) + G_i(t) + u_i(t) \right] \\
 &= -\sum_{i=1}^M \alpha_i |\Delta_i(t)| + \sum_{i=1}^M \text{sign}(\Delta_i(t)) G_i(t) + \sum_{i=1}^M \text{sign}(\Delta_i(t)) u_i(t) \\
 &\leq -\sum_{i=1}^M \alpha_i |\Delta_i(t)| + \sum_{i=1}^M |G_i(t)| + \sum_{i=1}^M \text{sign}(\Delta_i(t)) u_i(t)
 \end{aligned}$$

Using Lemma 8, we obtain

$$\begin{aligned}
 {}^C_{t_0}D^\omega V(\Delta(t)) &\leq -\sum_{i=1}^M \alpha_i |\Delta_i(t)| + \sum_{i=1}^M \sum_{r=1}^M (\tilde{\phi}_{ir} Q_r + \varepsilon \tilde{d}_{ir} Q'_r) |\Delta_r(t)| - \sum_{i=1}^M \kappa_i |\Delta_i(t)| \\
 &\quad - \sum_{i=1}^M |\text{sign}(\Delta_i(t))| \sum_{r=1}^M \theta_{ir} |\Delta_r(t - \tau(t))| \\
 &\quad - \sum_{i=1}^M \delta_i |\text{sign}(\Delta_i(t))| + \sum_{i=1}^M \sum_{r=1}^M \left[|\phi'_{ir} - \phi''_{ir}| S_r \right. \\
 &\quad \left. + \tilde{\psi}_{ir} Q_r |\Delta_r(t - \tau(t))| + |\psi'_{ir} - \psi''_{ir}| S_r + \varepsilon |\hat{d}_{ir} - d_{ir}| S'_r \right] \tag{20} \\
 &= \sum_{i=1}^M \left(-\alpha_i + \sum_{r=1}^M (\tilde{\phi}_{ri} Q_r + \varepsilon \tilde{d}_{ri} Q'_r) - \kappa_i \right) |\Delta_i(t)| \\
 &\quad + \sum_{i=1}^M \sum_{r=1}^M (\tilde{\psi}_{ir} Q_r - \theta_{ir}) |\Delta_r(t - \tau(t))| \\
 &\quad + \sum_{i=1}^M \left[\sum_{r=1}^M (|\phi'_{ri} - \phi''_{ri}| S_r + |\psi'_{ri} - \psi''_{ri}| S_r) + \varepsilon |\hat{d}_{ri} - d_{ri}| S'_r - \delta_i \right]
 \end{aligned}$$

While

$$\begin{cases}
 \kappa_i \geq -\alpha_i + \sum_{r=1}^M (\tilde{\phi}_{ri} Q_r + \varepsilon \tilde{d}_{ri} Q'_r), \\
 \theta_{ir} \geq \tilde{\psi}_{ir} Q_r, \\
 \delta_i > \sum_{r=1}^M (|\phi'_{ri} - \phi''_{ri}| S_r + |\psi'_{ri} - \psi''_{ri}| S_r + \varepsilon |\hat{d}_{ri} - d_{ri}| S'_r),
 \end{cases}$$

we obtain

$${}^C_{t_0}D^\omega V(\Delta(t)) \leq -\sum_{i=1}^M c_i |\text{sign}(\Delta_i(t))| \leq -\sum_{i=1}^M \min_{1 \leq i \leq M} \{c_i\} \tag{21}$$

where $c_i = \delta_i - \sum_{r=1}^M (|\phi'_{ri} - \phi''_{ri}| S_r + |\psi'_{ri} - \psi''_{ri}| S_r + \varepsilon |\hat{d}_{ri} - d_{ri}| S'_r) > 0$. According to Lemma 6, we obtain Equation (18). This completes the proof.

Remark 2. The feedback controller (16) includes two parts: $u_{i1}(t) = -\kappa_i \Delta_i(t) - \text{sign}(\Delta_i(t)) \sum_{r=1}^M \theta_{ir} |\Delta_r(t - \tau(t))|$ and $u_{i2}(t) = -\delta_i \text{sign}(\Delta_i(t))$. Here, the feedback controller $u_{i1}(t)$ can realize synchronization of FMCNNs (12) and (13); however, we cannot estimate the upper bound time for synchronization by the controller $u_{i1}(t)$. To realize the FMCNNs (12) and (13), we need the controller $u_{i2}(t)$.

Remark 3. In fact, the adaptive control method has strong robustness to external interference and unknown uncertainties and can identify the unknown parameters in the model according to the input and output data. In the control scheme (16), the feedback control parameters $-\kappa_i$ and θ_{ir} are not easy to choose, so the following considers the use of adaptive control to achieve finite-time synchronization of the driving response system.

Theorem 2. If Assumptions 1 and 2 hold, and control gains $\hat{\kappa}_i, \hat{\theta}_{ir}, \delta_i$ satisfy $\hat{\kappa}_i \geq -\alpha_i + \sum_{r=1}^M (\tilde{\phi}_{ri} Q_r + \varepsilon \tilde{d}_{ri} Q'_r), \theta_{ir} \geq \tilde{\psi}_{ir} Q_r, \hat{\theta}_{ir} \geq \tilde{\psi}_{ir} Q_r, \delta_i > \sum_{r=1}^M (|\phi'_{ri} - \phi''_{ri}| S_r + |\psi'_{ri} - \psi''_{ri}| S_r + \varepsilon |\hat{d}_{ri} - d_{ri}| S'_r), i, r = 1, 2, \dots, M$, then FMCNNs (12) and (13) can realize finite-time synchronization under the adaptive controller (17). Furthermore, the upper bound time for synchronization is calculated by (18).

Proof. Consider the Lyapunov function:

$$V(\Delta_i(t)) = \sum_{i=1}^M |\Delta_i(t)| + \sum_{i=1}^M \frac{1}{2\lambda_i} (\kappa_i(t) - \hat{\kappa}_i)^2 + \sum_{i=1}^M \sum_{r=1}^M \frac{1}{2\rho_i} (\theta_{ir}(t) - \hat{\theta}_{ir})^2 \tag{22}$$

□

Using Lemmas 3, 4, and 8, we calculate the fractional derivative of (22).

$$\begin{aligned} {}^C_{t_0} D^\omega V(\Delta(t)) &\leq \sum_{i=1}^M \text{sign}(\Delta_i(t)) {}^C_{t_0} D^\omega \Delta_i(t) \\ &\quad + \sum_{i=1}^M \frac{1}{\lambda_i} (\kappa_i(t) - \hat{\kappa}_i) {}^C_{t_0} D^\omega \kappa_i(t) + \sum_{i=1}^M \sum_{r=1}^M \frac{1}{\rho_i} (\theta_{ir}(t) - \hat{\theta}_{ir}) {}^C_{t_0} D^\omega \theta_{ir}(t) \end{aligned} \tag{23}$$

Combining (16), (20), and (23), one can obtain:

$$\begin{aligned} {}^C_{t_0} D^\omega V(\Delta(t)) &\leq \sum_{i=1}^M \left(-\alpha_i + \sum_{r=1}^M (\tilde{\phi}_{ri} Q_r + \varepsilon \tilde{d}_{ri} Q'_r) - \hat{\kappa}_i \right) |\Delta_i(t)| \\ &\quad + \sum_{i=1}^M \sum_{r=1}^M (\tilde{\psi}_{ir} Q_r - \hat{\theta}_{ir}) |\Delta_r(t - \tau(t))| \\ &\quad + \sum_{i=1}^M \left[\sum_{r=1}^M (|\phi'_{ri} - \phi''_{ri}| S_r + |\psi'_{ri} - \psi''_{ri}| S_r + \varepsilon |\hat{d}_{ri} - d_{ri}| S'_r - \delta_i) \right] \\ &\quad - \sum_{i=1}^M \frac{1}{2\lambda_i} (\kappa_i(t) - \hat{\kappa}_i)^2 - \sum_{i=1}^M \sum_{r=1}^M \frac{1}{2\rho_i} (\theta_{ir}(t) - \hat{\theta}_{ir})^2 \end{aligned} \tag{24}$$

While

$$\begin{cases} \hat{\kappa}_i \geq -\alpha_i + \sum_{r=1}^M (\tilde{\phi}_{ri} Q_r + \varepsilon \tilde{d}_{ri} Q'_r), \\ \hat{\theta}_{ir} \geq \tilde{\psi}_{ir} Q_r, \\ \delta_i > \sum_{r=1}^M (|\phi'_{ri} - \phi''_{ri}| S_r + |\psi'_{ri} - \psi''_{ri}| S_r + \varepsilon |\hat{d}_{ri} - d_{ri}| S'_r) \end{cases}$$

we obtain

$${}^C_{t_0} D^\omega V(\Delta(t)) \leq - \sum_{r=1}^M \left[(|\phi'_{ri} - \phi''_{ri}| S_r + |\psi'_{ri} - \psi''_{ri}| S_r + \varepsilon |\hat{d}_{ri} - d_{ri}| S'_r) \right] \leq - \sum_{i=1}^M \min_{1 \leq r \leq M} \{c_i\} \tag{25}$$

where $c_i = \delta_i - \sum_{r=1}^M (|\phi'_{ri} - \phi''_{ri}| S_r + |\psi'_{ri} - \psi''_{ri}| S_r + \varepsilon |\hat{d}_{ri} - d_{ri}| S'_r) > 0$. According to Lemma 6, we obtain Equation (18). This completes the proof.

Remark 4. It is worth noting that, theoretically, the upper bound T_{max} can be obtained based on Equation (17) in Theorem 1 or Theorem 2. One can see that T_{max} depends not only on the relevant initial state $V(t_0)$, but also on the fractional order ω and control gain δ_i .

Remark 5. It should be noted that, for finite-time synchronization, if the initial value of the system is unknown, the synchronization time of finite-time synchronization cannot be estimated. However, for fixed-time synchronization, even if the initial value of the system is unknown, the upper bound of the synchronization time can still be estimated. Therefore, we will study FMCNN fixed-time synchronization next.

4. Fixed-Time Synchronization Control

In this section, we discuss the fixed-time synchronization of FMCNNs (12) and (13). To achieve the fixed-time synchronization between (12) and (13), the controller is designed as:

$$u_i(t) = -\kappa_i \Delta_i(t) - \text{sign}(\Delta_i(t)) \left(\delta_i + \sum_{r=1}^M \theta_{ir} |\Delta_r(t - \tau(t))| + \eta_i ({}^C D_{t_0}^{\omega-1} |\Delta_i(t)|)^\iota \right) \tag{26}$$

where $\kappa_i > 0, \delta_i > 0, \theta_{ir} > 0, \eta_i > 0, \iota > 1$, and $\text{sign}(\cdot)$ is the symbolic function.

Theorem 3. If Assumptions 1 and 2 hold, and control gains $\kappa_i, \delta_i, \theta_{ir}$ satisfy $\kappa_i \geq -\alpha_i + \sum_{r=1}^M \tilde{\varphi}_{ir} Q_r, \delta_i > \sum_{r=1}^M (|\phi'_{ir} - \phi''_{ir}| S_r + |\psi'_{ir} - \psi''_{ir}| S_r), \theta_{ir} \geq \tilde{\psi}_{ir} Q_r, i, r = 1, 2, \dots, M$, then FMCNNs (12) and (13) can realize fixed-time synchronization under controller (26). Furthermore, the settling time can be calculated by:

$$T^* \leq T_{max} = \frac{1}{\Theta(\iota - 1)} \left(\frac{\Theta}{\Lambda M^{\iota-1}} \right)^{\frac{1}{\iota}} \tag{27}$$

where $\Lambda = \min_{1 \leq i \leq M} \eta_i, \Theta = \sum_{i=1}^M \min_{1 \leq i \leq M} \{c_i\}, \iota > 1$.

Proof. Consider the Lyapunov function:

$$V(\Delta(t)) = \sum_{i=1}^M {}^C D_{t_0}^{\omega-1} |\Delta_i(t)| \tag{28}$$

□

Obviously, $V(\Delta(t)) \geq 0$ and $V(\Delta(t)) = 0$ if and only if $\Delta(t) = 0$. Using Lemmas 1 and 2, we calculate the derivative of (28).

$$\begin{aligned} \dot{V}(\Delta(t)) &= {}^C D_{t_0}^{\omega} ({}^C D_{t_0}^{1-\omega} V(\Delta(t))) = {}^C D_{t_0}^{\omega} \left({}^C D_{t_0}^{1-\omega} \sum_{i=1}^M {}^C D_{t_0}^{\omega-1} |\Delta_i(t)| \right) \\ &= {}^C D_{t_0}^{\omega} \left({}^C D_{t_0}^{1-\omega} \left({}^C D_{t_0}^{\omega-1} \sum_{i=1}^M |\Delta_i(t)| \right) \right) \\ &= \sum_{i=1}^M {}^C D_{t_0}^{\omega} |\Delta_i(t)| \leq \sum_{i=1}^M \text{sign}(\Delta_i(t)) {}^C D_{t_0}^{\omega} \Delta_i(t) \end{aligned}$$

Similar to in the proof of Theorem 1, we choose to meet the conditions

$$\begin{cases} \kappa_i \geq -\alpha_i + \sum_{r=1}^M (\tilde{\varphi}_{ri} Q_r + \varepsilon \tilde{d}_{ri} Q'_r), \\ \theta_{ir} \geq \tilde{\psi}_{ir} Q_r, \\ \delta_i > \sum_{r=1}^M (|\phi'_{ri} - \phi''_{ri}| S_r + |\psi'_{ri} - \psi''_{ri}| S_r + \varepsilon |\hat{d}_{ri} - d_{ri}| S'_r), \end{cases}$$

and, according to Lemma 5, we obtain the following inequality:

$$\dot{V}(\Delta(t)) \leq - \sum_{i=1}^M \min_{1 \leq i \leq M} \{c_i\} - \sum_{i=1}^M \eta_i \left({}^C D^{\omega-1} |\Delta_i(t)| \right)^l$$

where $c_i = \delta_i - \sum_{r=1}^M (|\phi'_{ri} - \phi''_{ri}| S_r + |\psi'_{ri} - \psi''_{ri}| S_r + \varepsilon |\hat{d}_{ri} - d_{ri}| S_r) > 0$.

When $\Lambda = \min_{1 \leq i \leq M} \eta_i$, $\Theta = \sum_{i=1}^M \min_{1 \leq i \leq M} \{c_i\}$, we obtain:

$$\dot{V}(\Delta(t)) \leq -\Theta - \Lambda M^{1-l} (V(\Delta_i(t)))^l$$

Let $k = 1$ in Lemma 7. It is known that the origin is fixed-time stable, and the settling time T^* can be calculated by:

$$T^* \leq T_{\max} = \frac{1}{\Theta(l-1)} \left(\frac{\Theta}{\Lambda M^{1-l}} \right)^{\frac{1}{l}}$$

Remark 6. In this paper, the settling time T^* is calculated based on Lemma 7, and the algorithm of Lemma 7 itself is an optimization result. Actually, the estimation of time T^* is determined by the following equation:

$$\begin{aligned} T^* &\leq \int_0^{+\infty} \frac{1}{(\alpha x^\mu + \beta)^k} dx = \int_0^r \frac{1}{(\alpha x^\mu + \beta)^k} dx \\ &\quad + \int_r^{+\infty} \frac{1}{(\alpha x^\mu + \beta)^k} dx \\ &\leq \int_0^r \frac{1}{\beta^k} dx + \int_r^{+\infty} \frac{1}{\alpha^k x^{\mu k}} dx \\ &= \frac{r}{\beta^k} + \frac{1}{\alpha^k (\mu k - 1)} r^{1-\mu k} \end{aligned}$$

where r represents an arbitrary positive number. Let

$$W(r) = \frac{r}{\beta^k} + \frac{1}{\alpha^k (\mu k - 1)} r^{1-\mu k}$$

Then,

$$\dot{W}(r) = \frac{1}{\beta^k} + \frac{1}{\alpha^k (\mu k - 1)} r^{-\mu k}$$

which indicates that $W(r)$ can reach its minimum value, which can be calculated by the following formula:

$$\hat{W} = \frac{1}{\beta^k} \left(\frac{\beta}{\alpha} \right)^{\frac{1}{\mu}} \left(1 + \frac{1}{\mu k - 1} \right)$$

In order to refine the estimation of the settling time, it is imperative to select appropriate parameters α, β, k, μ in applications. Actually, if $\alpha > \beta$ and $\mu = \frac{\ln \frac{\beta}{\alpha}}{\ln \frac{\beta}{\alpha} + 1}$, the estimated value of T^* can be obtained using the following formula:

$$T^* \leq T_{\max} = \frac{\ln \frac{\beta}{\alpha}}{\beta} \left(\frac{\beta}{\alpha} \right)^{1 + \frac{1}{\ln \frac{\beta}{\alpha}}}$$

5. Numerical Simulations

To validate the obtained theoretical results, some numerical simulations will be provided next.

Example 1. Consider the drive system:

$$\begin{aligned}
 {}^C D^\omega p_i(t) = & -\alpha_i p_i(t) + \sum_{r=1}^3 \phi_{ir}(p_i(t)) f_r(p_r(t)) \\
 & + \sum_{r=1}^3 \psi_{ir}(p_i(t)) f_r(p_r(t - \tau(t))) + \varepsilon \sum_{r=1}^3 d_{ir} g_r(q_r(t)) + I_i, i = 1, 2, 3,
 \end{aligned}
 \tag{29}$$

The system parameter selection is as follows:

$$\begin{cases}
 \Gamma_1 = \Gamma_2 = \Gamma_3 = 1, \alpha_1 = \alpha_2 = \alpha_3 = 1, \varepsilon = 0.2, \omega = 0.95 \\
 \phi'_{11} = 2.0, \phi'_{12} = -1, \phi'_{13} = 1.8, \phi'_{21} = 0.8, \phi'_{22} = 1.5, \phi'_{23} = -1.0, \\
 \phi'_{31} = -1.1, \phi'_{32} = 2.0, \phi'_{33} = 1.5, \phi''_{11} = 2.2, \phi''_{12} = -1.2, \phi''_{13} = 2.0, \\
 \phi''_{21} = 1.0, \phi''_{22} = 1.8, \phi''_{23} = -1.5, \phi''_{31} = -1.0, \phi''_{32} = 1.7, \phi''_{33} = 2.0 \\
 \psi'_{11} = -2.0, \psi'_{12} = -0.5, \psi'_{13} = 1.5, \psi'_{21} = 2.5, \psi'_{22} = 5.0, \psi'_{23} = -2.5 \\
 \psi'_{31} = 2.4, \psi'_{32} = -2.0, \psi'_{33} = 4.5, \psi''_{11} = -1.5, \psi''_{12} = -1.0, \psi''_{13} = 2.0 \\
 \psi''_{21} = 2.2, \psi''_{22} = 4.5, \psi''_{23} = -3.0, \psi''_{31} = 2.0, \psi''_{32} = -18, \psi''_{33} = 5 \\
 d_{11} = 1.0, d_{12} = 2.0, d_{13} = 1.5, d_{21} = 2.0, d_{22} = 1.0, d_{23} = 0.5 \\
 d_{31} = 0.5, d_{32} = 2.0, d_{33} = 1.0, \hat{d}_{11} = 1.0, \hat{d}_{12} = 1.0, \hat{d}_{13} = 1.0 \\
 \hat{d}_{21} = 1.0, \hat{d}_{22} = 1.0, \hat{d}_{23} = 1.0, \hat{d}_{31} = 1.0, \hat{d}_{32} = 1.0, \hat{d}_{33} = 1.0
 \end{cases}
 \tag{30}$$

Let $f_i(p(t)) = \tanh(|p(t)|) - 1$, $g_i(p(t)) = \tanh(p(t))$, $I_i = 0.1$, $S_i = S'_i = 1$, $Q_i = Q'_i = 1, i = 1, 2, 3$. $\tau(t) = \frac{e^t}{1+e^t}$. The initial values of system (29) are $\zeta_1(v) = 0.3$, $\zeta_2(v) = 0.6$, $\zeta_3(v) = -0.3, v \in [-\tau(t), 0]$.

The response system is:

$$\begin{aligned}
 {}^C D^\omega q_i(t) = & -\alpha_i q_i(t) + \sum_{r=1}^3 \phi_{ir}(q_i(t)) f_r(q_r(t)) \\
 & + \sum_{r=1}^3 \psi_{ir}(q_i(t)) f_r(q_r(t - \tau(t))) + \varepsilon \sum_{r=1}^3 \hat{d}_{ir} g_r(p_r(t)) + I_i + u_i(t), i = 1, 2, 3.
 \end{aligned}
 \tag{31}$$

The parameters are the same as in the system (29). The initial values of system (31) are $\zeta_1(v) = 0.3, \zeta_2(v) = -0.6, \zeta_3(v) = 0.3, v \in [-\tau(t), 0]$.

According to Theorem 1, control parameters $\kappa_i, \delta_i, \theta_{ir}, i, r = 1, 2, 3$ should satisfy

$$\begin{aligned}
 \kappa_i & \geq -\alpha_i + \sum_{r=1}^M (\tilde{\phi}_{ri} Q_r + \varepsilon \tilde{d}_{ri} Q'_r), \\
 \theta_{ir} & \geq \tilde{\psi}_{ir} Q_r, \\
 \delta_i & > \sum_{r=1}^M (|\phi'_{ri} - \phi''_{ri}| S_r + |\psi'_{ri} - \psi''_{ri}| S_r + \varepsilon |\hat{d}_{ri} - d_{ri}| S'_r),
 \end{aligned}$$

Here, we choose

$$\begin{cases}
 \kappa_1 = 5.5, \kappa_2 = 6.2, \kappa_3 = 6.7, \\
 \delta_1 = 3.0, \delta_2 = 2.5, \delta_3 = 3.5 \\
 \theta_{11} = 3.0, \theta_{12} = 1.3, \theta_{13} = 2.5, \\
 \theta_{21} = 2.6, \theta_{22} = 5.2, \theta_{23} = 3.1, \\
 \theta_{31} = 2.5, \theta_{32} = 2.1, \theta_{33} = 5.1,
 \end{cases}
 \tag{32}$$

Figure 1 illustrates the phase trajectories of system (29) in two-dimensional state space without controller. Figure 2 show the state trajectories of systems (29) and (31) without controller. Figure 2 indicates that they have not reached synchronization without controller. Figure 3 show the state trajectories of systems (29) and (31) with controller. Figure 3 shows

the state trajectories of the error system with controller. Figure 3 indicates that they can achieve synchronization within a finite time under this controller (16). Furthermore, according to Theorem 1, $T_{\max} = 4.2117$ can be computed using Formula (18). This sufficiently confirms that Theorem 2 is effective.

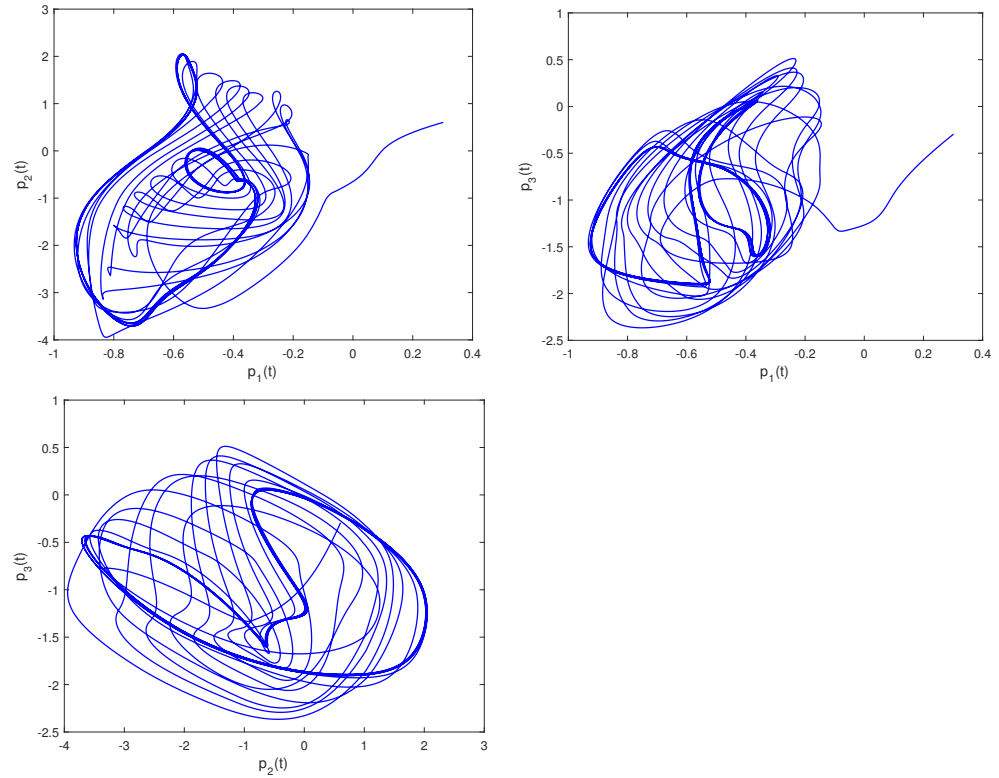


Figure 1. Phase trajectories of (29) in two-dimensional spaces.

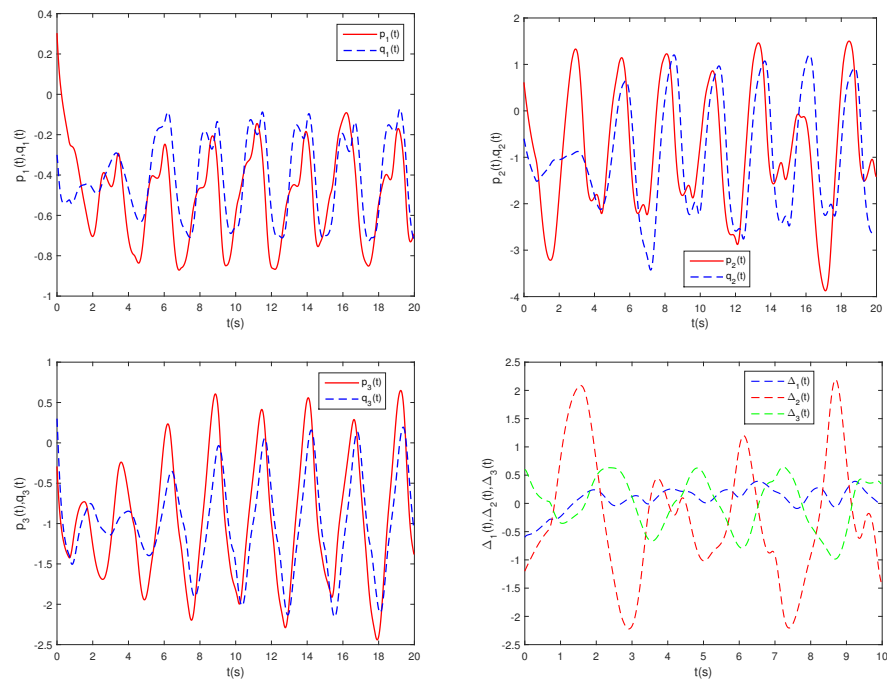


Figure 2. State trajectories of $p_i(t)$, $q_i(t)$, and $\Delta_i(t)$ without controller.

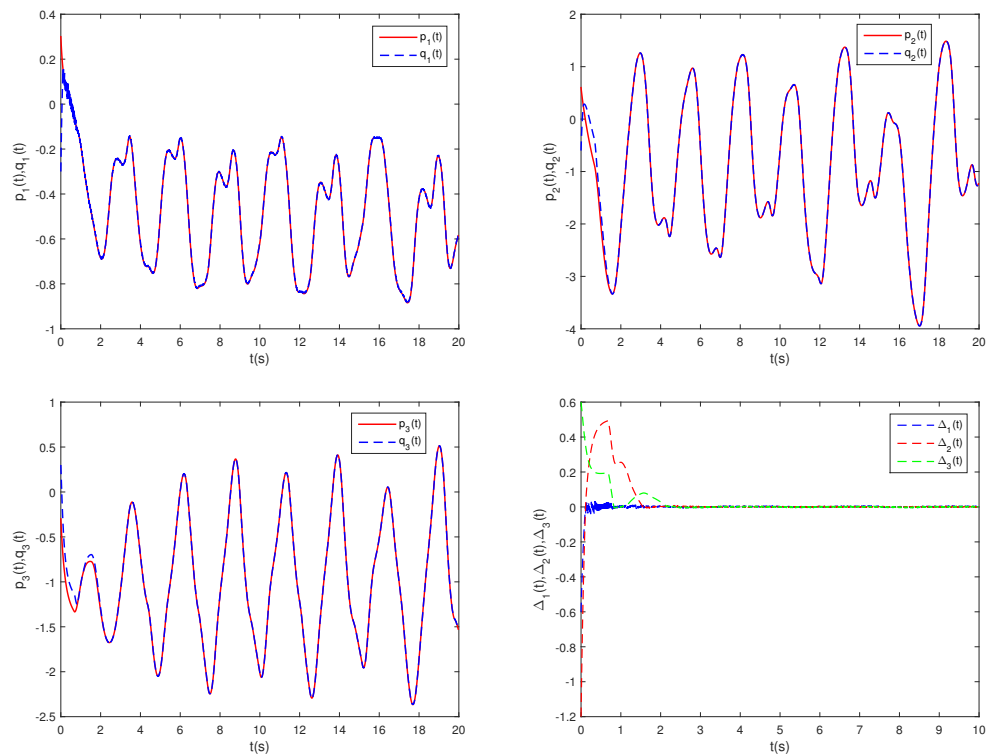


Figure 3. State trajectories of $p_i(t)$, $q_i(t)$, and $\Delta_i(t)$ with controller.

Example 2. For system (29), the system parameter selection is as follows:

$$\left\{ \begin{array}{l}
 \Gamma_1 = \Gamma_2 = \Gamma_3 = 1, \alpha_1 = \alpha_2 = \alpha_3 = 1, \varepsilon = 0.2, \omega = 0.9 \\
 \phi'_{11} = 1.8, \phi'_{12} = -1, \phi'_{13} = 1.6, \phi'_{21} = 0.8, \phi'_{22} = 1.1, \phi'_{23} = -1.0, \\
 \phi'_{31} = -1.1, \phi'_{32} = 2.0, \phi'_{33} = 1.5, \phi''_{11} = 2.0, \phi''_{12} = -0.9, \phi''_{13} = 1.8, \\
 \phi''_{21} = 1.1, \phi''_{22} = 1.2, \phi''_{23} = -1.3, \phi''_{31} = -1.2, \phi''_{32} = 1.7, \phi''_{33} = 2.1 \\
 \psi'_{11} = -1.1, \psi'_{12} = -0.5, \psi'_{13} = 0.8, \psi'_{21} = 1.4, \psi'_{22} = 1.5, \psi'_{23} = -0.5 \\
 \psi'_{31} = 1.4, \psi'_{32} = -1.0, \psi'_{33} = 1.2, \psi''_{11} = -0.8, \psi''_{12} = -0.7, \psi''_{13} = 1.2 \\
 \psi''_{21} = 1.1, \psi''_{22} = 0.5, \psi''_{23} = -0.6, \psi''_{31} = 1.7, \psi''_{32} = -1.2, \psi''_{33} = 1.5 \\
 d_{11} = 1.0, d_{12} = 2.0, d_{13} = 1, d_{21} = 1.5, d_{22} = 1.0, d_{23} = 0.5 \\
 d_{31} = 0.5, d_{32} = 1, d_{33} = 1.0, \hat{d}_{11} = 0.5, \hat{d}_{12} = 0.5, \hat{d}_{13} = 0.5 \\
 \hat{d}_{21} = 0.5, \hat{d}_{22} = 0.5, \hat{d}_{23} = 0.5, \hat{d}_{31} = 0.5, \hat{d}_{32} = 0.5, \hat{d}_{33} = 0.5
 \end{array} \right. \quad (33)$$

Let $f_i(p(t)) = \tanh(|p(t)|) - 1$, $g_i(p(t)) = \tanh(p(t))$, $I_i = 0.1$, $S_i = S'_i = 1$, $Q_i = Q'_i = 1, i = 1, 2, 3$. $\tau(t) = \frac{e^t}{1+e^t}$. The initial values of system (29) are $\zeta_1(v) = 1$, $\zeta_2(v) = 0.6$, $\zeta_3(v) = -0.2$, $v \in [-\tau(t), 0]$.

The parameters of response system (31) are the same as in system (29). The initial values of system (31) are $\tilde{\zeta}_1(v) = -1$, $\tilde{\zeta}_2(v) = -0.6$, $\tilde{\zeta}_3(v) = 0.8, v \in [-\tau(t), 0]$.

According to Theorem 2, control gains $\kappa_i, \delta_i, \theta_{ir}, \lambda_i, \rho_i, i, r = 1, 2, 3$ should satisfy

$$\begin{aligned} \hat{\kappa}_i &\geq -\alpha_i + \sum_{r=1}^M (\tilde{\phi}_{ri} Q_r + \varepsilon \tilde{d}_{ri} Q'_r), \\ \hat{\theta}_{ir} &\geq \tilde{\psi}_{ir} Q_r, \\ \delta_i &> \sum_{r=1}^M (|\phi'_{ri} - \phi''_{ri}| S_r + |\psi'_{ri} - \psi''_{ri}| S_r + \varepsilon |\hat{d}_{ri} - d_{ri}| S'_r) \end{aligned}$$

Here, we choose

$$\begin{cases} \hat{\kappa}_1 = 4.4, \hat{\kappa}_2 = 5.8, \hat{\kappa}_3 = 6.5, \\ \hat{\theta}_{11} = 2.0, \hat{\theta}_{12} = 1.0, \hat{\theta}_{13} = 2.3, \\ \hat{\theta}_{21} = 1.5, \hat{\theta}_{22} = 4.8, \hat{\theta}_{23} = 4.0, \\ \hat{\theta}_{31} = 3.6, \hat{\theta}_{32} = 2.8, \hat{\theta}_{33} = 5.2, \\ \delta_1 = 2.8, \delta_2 = 3.0, \delta_3 = 3.5, \\ \lambda_1 = \lambda_2 = \lambda_3 = 1, \rho_1 = \rho_2 = \rho_3 = 1 \end{cases} \tag{34}$$

Let $\kappa_i(0) = 1, \theta_{ir}(0) = 0.1, i, r = 1, 2, 3$.

Figure 4 illustrates the phase trajectories of system (29) in two-dimensional state space without controller. Figure 5 show the state trajectories of systems (29) and (31) without controller. Figure 5 indicates that they have not reached synchronization without controller. Figure 6 show the state trajectories of systems (29) and (31) with controller. Figure 6 shows the state trajectories of the error system with controller. Figure 6 indicates that they can achieve synchronization within a finite time under this controller (17). Furthermore, according to Theorem 2, $T_{\max} = 4.8839$ can be computed using Formula (18). Figures 7 and 8 indicate the time response trajectory of the adaptive control gains $\kappa_i(t)$ and $\theta_{ir}(t), (i, r = 1, 2, 3)$. This clearly indicates that the adaptive control gains $\kappa_i(t), \theta_{ir}(t)$ converge to some values within a finite time. This sufficiently confirms that Theorem 2 is effective.

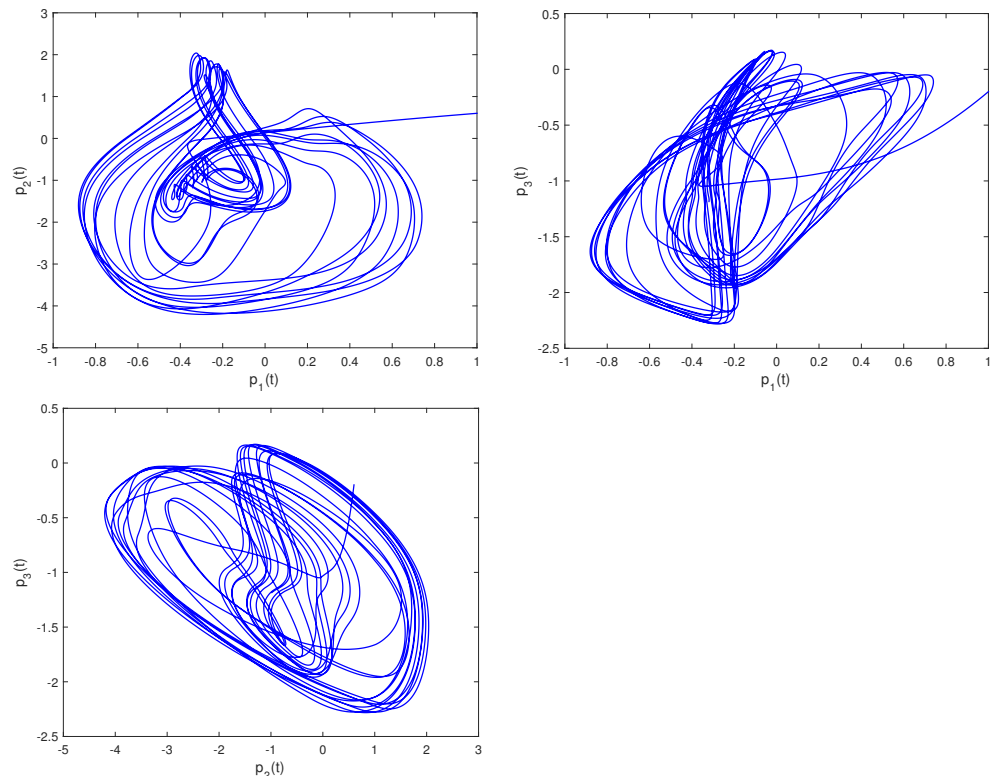


Figure 4. Phase trajectories of (29) in two-dimensional spaces.

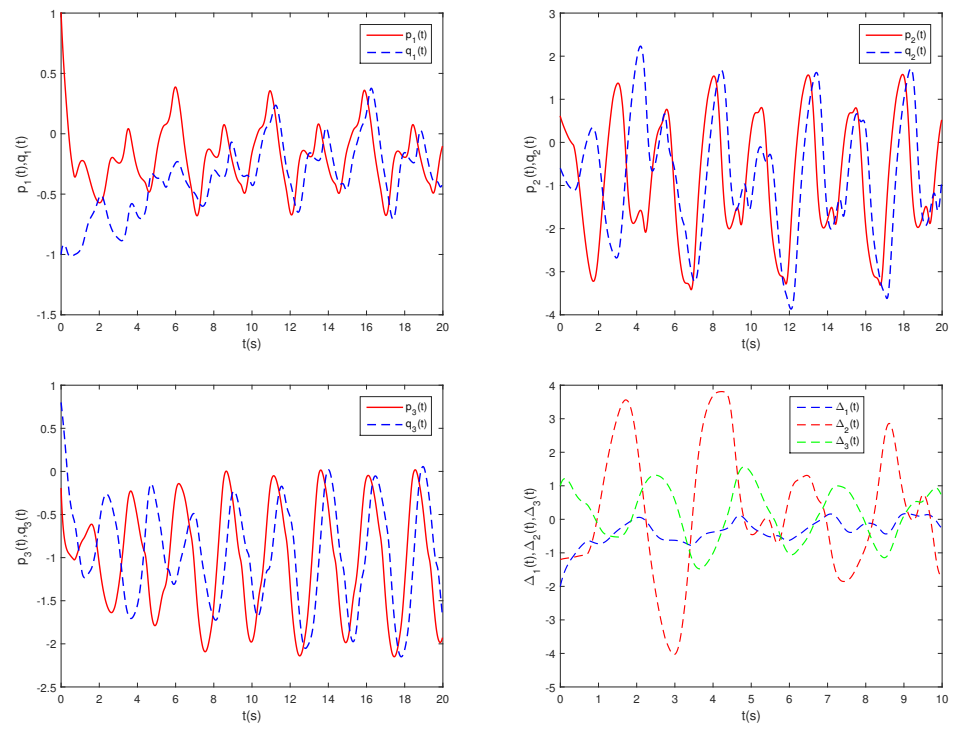


Figure 5. State trajectories of $p_i(t)$, $q_i(t)$, and $\Delta_i(t)$ without controller.

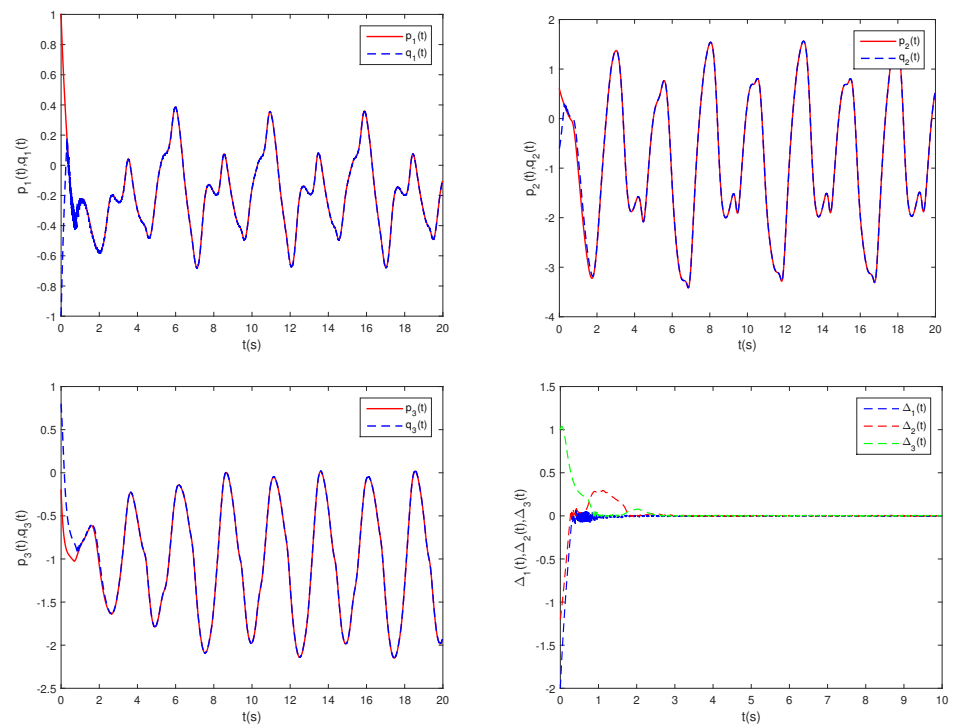


Figure 6. State trajectories of $p_i(t)$, $q_i(t)$, and $\Delta_i(t)$ with controller.

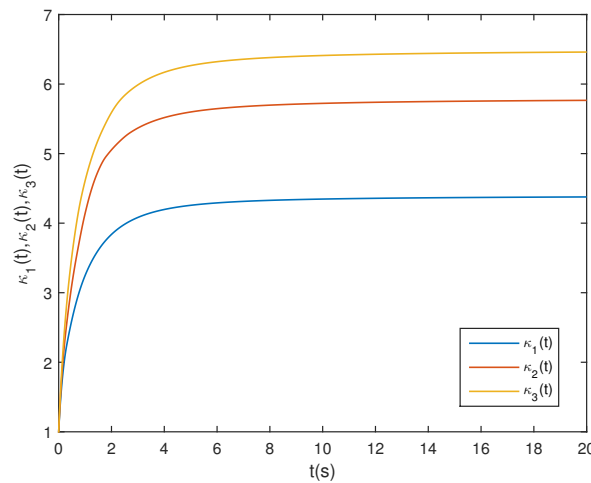


Figure 7. State trajectories of control gains $\kappa_i(t), i = 1, 2, 3$.

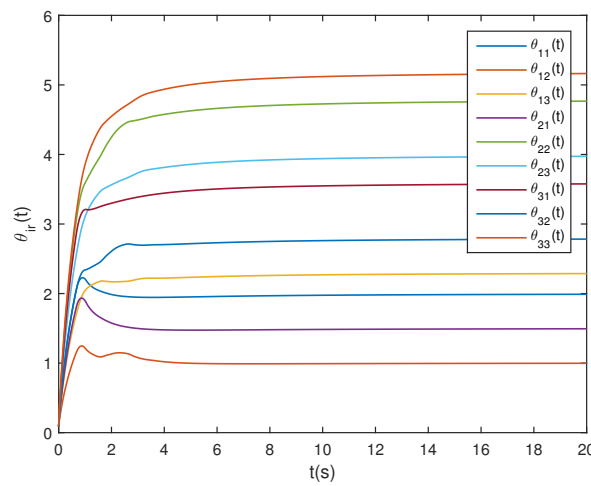


Figure 8. State trajectories of control gains $\theta_{ir}(t), i, r = 1, 2, 3$.

Example 3. For system (29), the system parameter selection is as follows:

$$\begin{cases}
 \Gamma_1 = \Gamma_2 = \Gamma_3 = 1, \alpha_1 = \alpha_2 = \alpha_3 = 1, \varepsilon = 0.2, \omega = 0.95 \\
 \phi'_{11} = 2.5, \phi'_{12} = -2, \phi'_{13} = -3, \phi'_{21} = 2.2, \phi'_{22} = -1.8, \phi'_{23} = 2.4, \\
 \phi'_{31} = 2.2, \phi'_{32} = -2.4, \phi'_{33} = 3.6, \phi''_{11} = 2.6, \phi''_{12} = -2.2, \phi''_{13} = -3.4, \\
 \phi''_{21} = 2.6, \phi''_{22} = -2.2, \phi''_{23} = 2.2, \phi''_{31} = 2.8, \phi''_{32} = -2.2, \phi''_{33} = 3.2 \\
 \psi'_{11} = -2.0, \psi'_{12} = -0.5, \psi'_{13} = 1.5, \psi'_{21} = 2.5, \psi'_{22} = 5.0, \psi'_{23} = -2.5 \\
 \psi'_{31} = 2.4, \psi'_{32} = -2.0, \psi'_{33} = 4.5, \psi''_{11} = -1.5, \psi''_{12} = -1.0, \psi''_{13} = 2.0 \\
 \psi''_{21} = 2.2, \psi''_{22} = 4.5, \psi''_{23} = -3.0, \psi''_{31} = 2.0, \psi''_{32} = -18, \psi''_{33} = 5.0 \\
 d_{11} = 1.0, d_{12} = 2.0, d_{13} = 1.5, d_{21} = 2.0, d_{22} = 1.0, d_{23} = 0.5 \\
 d_{31} = 0.5, d_{32} = 2, d_{33} = 1.0, \hat{d}_{11} = 1.0, \hat{d}_{12} = 1.0, \hat{d}_{13} = 1.0 \\
 \hat{d}_{21} = 1.0, \hat{d}_{22} = 1.0, \hat{d}_{23} = 1.0, \hat{d}_{31} = 1.0, \hat{d}_{32} = 1.0, \hat{d}_{33} = 1.0
 \end{cases} \tag{35}$$

Let $f_i(p(t)) = \tanh(|p(t)|) - 1, g_i(p(t)) = \tanh(p(t)), I_i = 0.1. \tau(t) = \frac{e^t}{1+e^t}$. The initial values of system (29) are $\zeta_1(v) = 0.2, \zeta_2(v) = -0.4, \zeta_3(v) = 0.6, v \in [-\tau(t), 0]$.

The parameters of response system (31) are the same as in system (29). The initial values of system (31) are $\check{\zeta}_1(v) = -0.2, \check{\zeta}_2(v) = 0.4, \check{\zeta}_3(v) = -0.6, v \in [-\tau(t), 0]$.

According to Theorem 3, control gains $\kappa_i, \delta_i, \theta_{ir}, \eta_i, i, r = 1, 2, 3$ should satisfy

$$\begin{aligned} \kappa_i &\geq -\alpha_i + \sum_{r=1}^M (\tilde{\phi}_{ri} Q_r + \varepsilon \tilde{d}_{ri} Q'_r), \\ \theta_{ir} &\geq \tilde{\psi}_{ir} Q_r, \\ \delta_i &> \sum_{r=1}^M (|\phi'_{ri} - \phi''_{ri}| S_r + |\psi'_{ri} - \psi''_{ri}| S_r + \varepsilon |\hat{d}_{ri} - d_{ri}| S'_r), \end{aligned}$$

Here, we choose

$$\begin{cases} \kappa_1 = 5.5, \kappa_2 = 6.2, \kappa_3 = 6.7, \\ \delta_1 = 2.5, \delta_2 = 2.6, \delta_3 = 3.5 \\ \theta_{11} = 2.5, \theta_{12} = 1.5, \theta_{13} = 2.5, \\ \theta_{21} = 2.6, \theta_{22} = 5.4, \theta_{23} = 3.2, \\ \theta_{31} = 2.8, \theta_{32} = 2.2, \theta_{33} = 5.2, \\ \eta_1 = \eta_2 = \eta_3 = 0.5, \iota = 1.5 \end{cases} \tag{36}$$

Figure 9 illustrates the phase trajectories of system (29) in two-dimensional state space without controller. Figure 10 show the state trajectories of systems (29) and (31) without controller. Figure 10 indicates that they have not reached synchronization without controller. Figure 11 show the state trajectories of systems (29) and (31) with controller. Figure 11 shows the state trajectories of the error system with controller. Figure 11 indicates that they can achieve synchronization before a fixed time point under this controller (26). Furthermore, according to Theorem 3, $T_{\max} = 4.7425$ can be computed using Formula (27). This sufficiently confirms that Theorem 3 is effective.

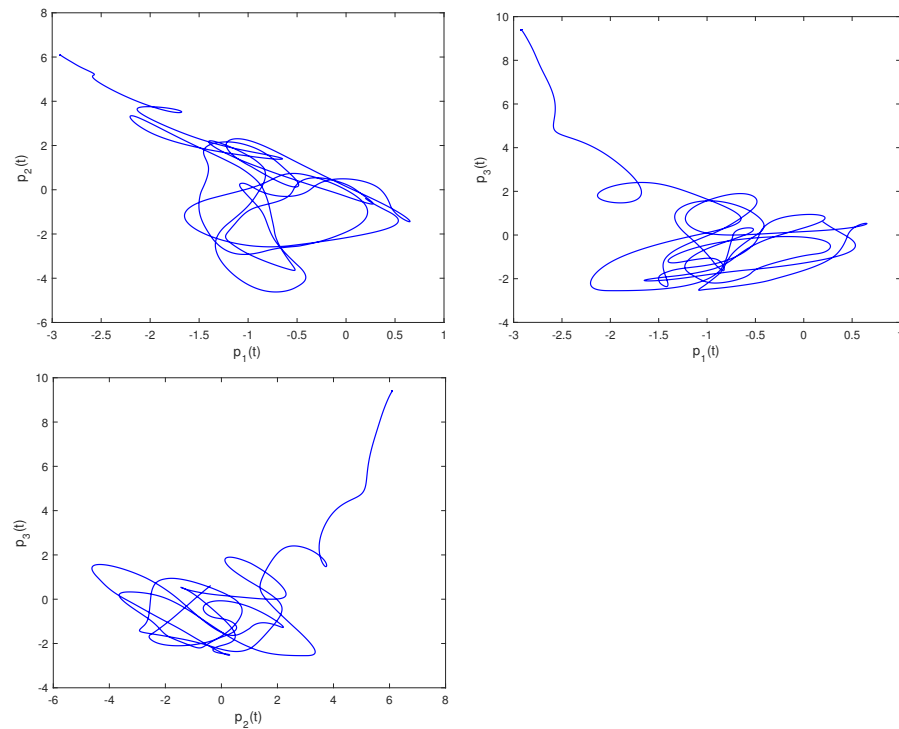


Figure 9. Phase trajectories of (29) in two-dimensional spaces.

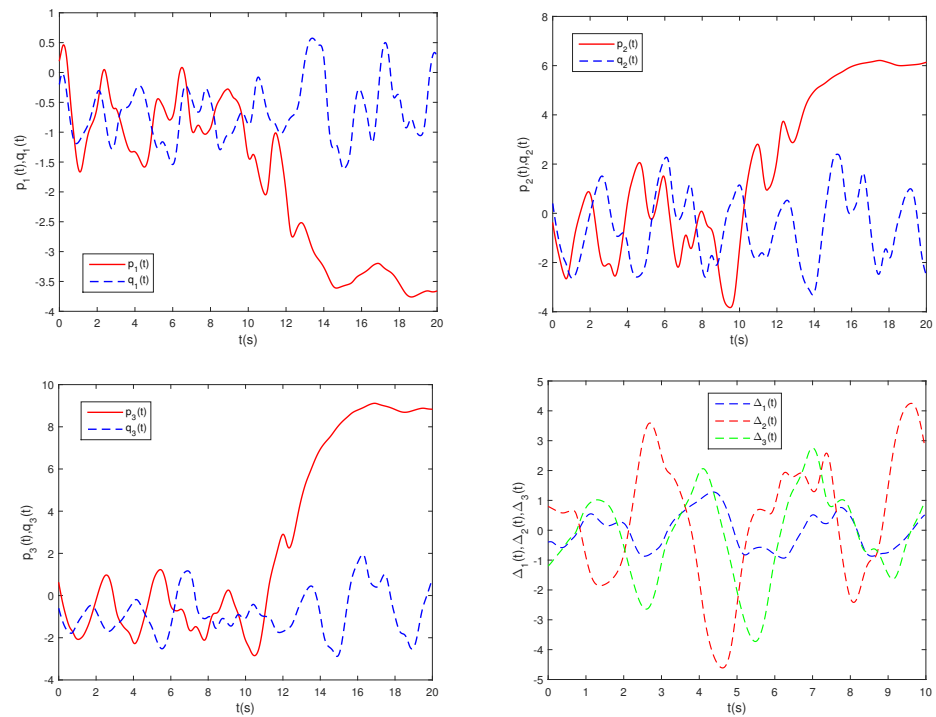


Figure 10. State trajectories of $p_i(t)$, $q_i(t)$, and $\Delta_i(t)$ without controller.

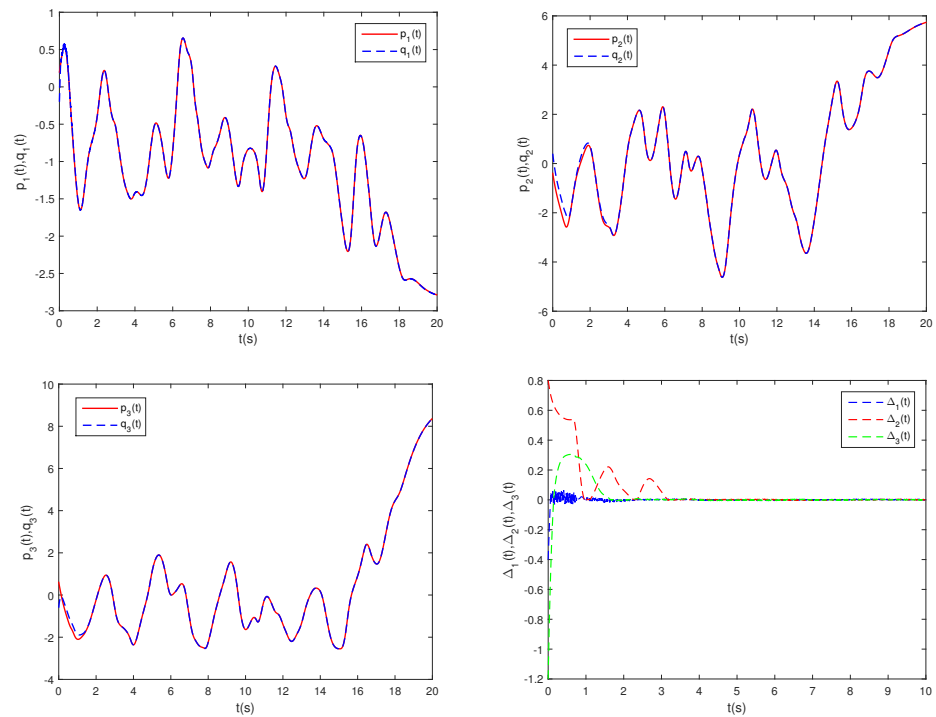


Figure 11. State trajectories of $p_i(t)$, $q_i(t)$, and $\Delta_i(t)$ with controller.

6. Conclusions

This paper explores the finite-time adaptive synchronization and fixed-time synchronization of FMCNNs with TVD. Utilizing the properties and principles of fractional order, we introduce a novel lemma. Based on this lemma and various analysis techniques, we establish new criteria to guarantee FTAS and FDTS of FMCNNs with TVD through the implementation of a delay-dependent feedback controller and fractional-order adaptive

controller. Additionally, we estimate the upper bound of the synchronization setting time. Finally, numerical simulations are conducted to confirm the validity of the finite-time and fixed-time stability theorems. The results of the numerical simulations substantiate the validity of the conclusions presented in this paper. In future work, based on the research results of this article, we will further study the synchronization problem of discrete-time FMCNNs with TVD.

Author Contributions: Conceptualization, methodology, writing—original draft preparation, Y.L. and Y.S.; writing—review and editing, numerical simulation, Y.L.; project administration, Y.S. All authors have read and agreed to the published version of the manuscript.

Funding: This work was partly supported by the Natural Science Foundation of Anhui Province (2008085MF200), the Program for Innovative Research Team in Universities of Anhui Province (2022AH010085), the University Natural Science Foundation of Anhui Province (KJ2021A0970), the National Natural Science Foundation of China (61403157), and the Research and Development Plan Project Foundation of Huainan (2021A248).

Data Availability Statement: The data presented in this study are available in the article.

Acknowledgments: The authors would like to thank the anonymous referees and reviewers for their helpful comments, which have significantly improved the quality of the presentation.

Conflicts of Interest: The authors declare no conflicts of interest.

References

1. Yang, X.; Ho, D.W. Synchronization of delayed memristive neural networks: Robust analysis approach. *IEEE Trans. Cybern.* **2015**, *46*, 3377–3387. [[CrossRef](#)]
2. Wen, S.; Zeng, Z.; Huang, T.; Zhang, Y. Exponential adaptive lag synchronization of memristive neural networks via fuzzy method and applications in pseudorandom number generators. *IEEE Trans. Fuzzy Syst.* **2013**, *22*, 1704–1713. [[CrossRef](#)]
3. Hu, X.; Feng, G.; Duan, S.; Liu, L. A memristive multilayer cellular neural network with applications to image processing. *IEEE Trans. Neural Netw. Learn. Syst.* **2016**, *28*, 1889–1901. [[CrossRef](#)]
4. Chua, L. Memristor—the missing circuit element. *IEEE Trans. Circuit Theory* **1971**, *18*, 507–519. [[CrossRef](#)]
5. Ali, M.S.; Hymavathi, M.; Senan, S.; Shekher, V.; Arik, S. Global asymptotic synchronization of impulsive fractional-order complex-valued memristor-based neural networks with time varying delays. *Commun. Nonlinear Sci. Numer. Simul.* **2019**, *78*, 104869.
6. Li, N.; Zheng, W.X. Synchronization criteria for inertial memristor-based neural networks with linear coupling. *Neural Netw.* **2018**, *106*, 260–270. [[CrossRef](#)]
7. Wu, K.; Jian, J. Non-reduced order strategies for global dissipativity of memristive neutral-type inertial neural networks with mixed time-varying delays. *Neurocomputing* **2021**, *436*, 174–183. [[CrossRef](#)]
8. Zhang, T.; Jian, J. New results on synchronization for second-order fuzzy memristive neural networks with time-varying and infinite distributed delays. *Knowl.-Based Syst.* **2021**, *230*, 107397. [[CrossRef](#)]
9. Sun, Y.; Liu, Y.; Liu, L. Asymptotic and finite-time synchronization of fractional-order memristor-based inertial neural networks with time-varying delay. *Fractal Fract.* **2022**, *6*, 350. [[CrossRef](#)]
10. Zhang, X.; Jiang, W. Construction of flux-controlled memristor and circuit simulation based on smooth cellular neural networks module. *IET Circuits Devices Syst.* **2018**, *12*, 263–270. [[CrossRef](#)]
11. Ascoli, A.; Messaris, I.; Tetzlaff, R.; Chua, L.O. Theoretical foundations of memristor cellular nonlinear networks: Stability analysis with dynamic memristors. *IEEE Trans. Circuits Syst. I Regul. Pap.* **2019**, *67*, 1389–1401. [[CrossRef](#)]
12. Song, C.; Cao, J. Dynamics in fractional-order neural networks. *Neurocomputing* **2014**, *142*, 494–498. [[CrossRef](#)]
13. Wang, H.; Yu, Y.; Wen, G. Stability analysis of fractional-order Hopfield neural networks with time delays. *Neural Netw.* **2014**, *55*, 98–109. [[CrossRef](#)]
14. Ma, Z.; Ma, H. Adaptive fuzzy backstepping dynamic surface control of strict-feedback fractional-order uncertain nonlinear systems. *IEEE Trans. Fuzzy Syst.* **2020**, *28*, 122–133. [[CrossRef](#)]
15. Zhang, Q.; Lu, J. Bounded real lemmas for singular fractional-order systems: The $1 < \alpha < 2$ case. *IEEE Trans. Circuits Syst. II Express Briefs* **2021**, *68*, 732–736.
16. Shafiya, M.; Nagamani, G.; Dafik, D. Global synchronization of uncertain fractional-order BAM neural networks with time delay via improved fractional-order integral inequality. *Math. Comput. Simul.* **2022**, *191*, 168–186. [[CrossRef](#)]
17. Yan, S.; Gu, Z.; Nguang, S. Memory-event-triggered H_∞ output control of neural networks with mixed delays. *IEEE Trans. Neural Netw. Learn. Syst.* **2022**, *33*, 6905–6915. [[CrossRef](#)] [[PubMed](#)]
18. Jian, J.; Duan, L. Finite-time synchronization for fuzzy neutral-type inertial neural networks with time-varying coefficients and proportional delays. *Fuzzy Sets Syst.* **2020**, *381*, 51–67. [[CrossRef](#)]

19. Li, H.L.; Zhang, L.; Hu, C.; Jiang, H.; Cao, J. Global Mittag-Leffler synchronization of fractional-order delayed quaternion-valued neural networks: Direct quaternion approach. *Appl. Math. Comput.* **2020**, *373*, 125020. [[CrossRef](#)]
20. Zhang, H.; Cheng, J.; Zhang, H.; Zhang, W.; Cao, J. Quasi-uniform synchronization of Caputo type fractional neural networks with leakage and discrete delays. *Chaos Solitons Fractals* **2021**, *152*, 111432. [[CrossRef](#)]
21. Tong, D.; Zhang, L.; Zhou, W.; Zhou, J.; Xu, Y. Asymptotical synchronization for delayed stochastic neural networks with uncertainty via adaptive control. *Int. J. Control Autom. Syst.* **2016**, *14*, 706–712. [[CrossRef](#)]
22. Xiong, X.; Zhang, Z. Asymptotic synchronization of conformable fractional-order neural networks by L'Hopital's rule. *Chaos Solitons Fractals* **2023**, *173*, 113665. [[CrossRef](#)]
23. Guo, Z.; Gong, S.; Yang, S.; Huang, T. Global exponential synchronization of multiple coupled inertial memristive neural networks with time-varying delay via nonlinear coupling. *Neural Netw.* **2018**, *108*, 260–271. [[CrossRef](#)]
24. Zhang, T.; Jian, J. Quantized intermittent control tactics for exponential synchronization of quaternion-valued memristive delayed neural networks. *ISA Trans.* **2022**, *126*, 288–299. [[CrossRef](#)] [[PubMed](#)]
25. Zheng, C.; Cao, J. Robust synchronization of coupled neural networks with mixed delays and uncertain parameters by intermittent pinning control. *Neurocomputing* **2014**, *141*, 153–159. [[CrossRef](#)]
26. Duan, L.; Wei, H.; Huang, L. Finite-time synchronization of delayed fuzzy cellular neural networks with discontinuous activations. *Fuzzy Sets Syst.* **2019**, *361*, 56–70. [[CrossRef](#)]
27. Li, H.L.; Cao, J.; Jiang, H.; Alsaedi, A. Graph theory-based finite-time synchronization of fractional-order complex dynamical networks. *J. Frankl. Inst.* **2018**, *355*, 5771–5789. [[CrossRef](#)]
28. Lu, J.; Guo, Y.; Ji, Y.; Fan, S. Finite-time synchronization for different dimensional fractional-order complex dynamical networks. *Chaos Solitons Fractals* **2020**, *130*, 109433. [[CrossRef](#)]
29. Shanmugam, S.; Narayanan, G.; Rajagopal, K.; Ali, M.S. Finite-time synchronization of complex-valued neural networks with reaction-diffusion terms: An adaptive intermittent control approach. *Neural Comput. Appl.* **2024**, *36*, 7389–7404. [[CrossRef](#)]
30. He, X.; Wang, Y.; Li, T.; Kang, R.; Zhao, Y. Novel Controller Design for Finite-Time Synchronization of Fractional-Order Nonidentical Complex Dynamical Networks under Uncertain Parameters. *Fractal Fract.* **2024**, *8*, 155. [[CrossRef](#)]
31. Xiao, J.; Wu, L.; Wu, A.; Zeng, Z.; Zhang, Z. Novel controller design for finite-time synchronization of fractional-order memristive neural networks. *Neurocomputing* **2022**, *512*, 494–502. [[CrossRef](#)]
32. Duan, L.; Li, J. Fixed-time synchronization of fuzzy neutral-type BAM memristive inertial neural networks with proportional delays. *Inf. Sci.* **2021**, *576*, 522–541. [[CrossRef](#)]
33. Polyakov, A. Nonlinear feedback design for fixed-time stabilization of linear control systems. *IEEE Trans. Autom. Control* **2011**, *57*, 2106–2110. [[CrossRef](#)]
34. Cheng, Y.; Hu, T.; Xu, W.; Zhang, X.; Zhong, S. Fixed-time synchronization of fractional-order complex-valued neural networks with time-varying delay via sliding mode control. *Neurocomputing* **2022**, *505*, 339–352. [[CrossRef](#)]
35. Sun, Y.; Liu, Y. Fixed-time synchronization of delayed fractional-order memristor-based fuzzy cellular neural networks. *IEEE Access* **2020**, *8*, 165951–165962. [[CrossRef](#)]
36. Li, X.; Fang, J.A.; Zhang, W.; Li, H. Finite-time synchronization of fractional-order memristive recurrent neural networks with discontinuous activation functions. *Neurocomputing* **2018**, *316*, 284–293. [[CrossRef](#)]
37. Li, J.; Jiang, H.; Hu, C.; Alsaedi, A. Finite/fixed-time synchronization control of coupled memristive neural networks. *J. Frankl. Inst.* **2019**, *356*, 9928–9952. [[CrossRef](#)]
38. Li, X.; Zhang, W.; Fang, J. Finite-time synchronization of memristive neural networks with discontinuous activation functions and mixed time-varying delays. *Neurocomputing* **2019**, *340*, 99–109. [[CrossRef](#)]
39. Zhang, Y.; Deng, S. Finite-time projective synchronization of fractional-order complex-valued memristor-based neural networks with delay. *Chaos Solitons Fractals* **2019**, *128*, 176–190. [[CrossRef](#)]
40. Guo, Z. Finite-time synchronization of inertial memristive neural networks with time delay via delay-dependent control. *Neurocomputing* **2018**, *293*, 100–107. [[CrossRef](#)]
41. Wei, F.; Chen, G.; Zeng, Z.; Gunasekaran, N. Finite/fixed-time synchronization of inertial memristive neural networks by interval matrix method for secure communication. *Neural Netw.* **2023**, *167*, 168–182. [[CrossRef](#)] [[PubMed](#)]
42. Gong, S.; Guo, Z.; Wen, S. Finite-time synchronization of TS fuzzy memristive neural networks with time delay. *Fuzzy Sets Syst.* **2023**, *459*, 67–81. [[CrossRef](#)]
43. Zhao, F.; Jian, J.; Wang, B. Finite-time synchronization of fractional-order delayed memristive fuzzy neural networks. *Fuzzy Sets Syst.* **2023**, *467*, 108578. [[CrossRef](#)]
44. Arslan, E.; Narayanan, G.; Ali, M.S.; Arik, S.; Saroha, S. Controller design for finite-time and fixed-time stabilization of fractional-order memristive complex-valued BAM neural networks with uncertain parameters and time-varying delays. *Neural Netw.* **2020**, *130*, 60–74. [[CrossRef](#)] [[PubMed](#)]
45. Wang, W.; Jia, X.; Wang, Z.; Luo, X.; Li, L.; Kurths, J.; Yuan, M. Fixed-time synchronization of fractional order memristive MAM neural networks by sliding mode control. *Neurocomputing* **2020**, *401*, 364–376. [[CrossRef](#)]
46. Xiao, J.; Hu, Y.; Zeng, Z.; Wu, A.; Wen, S. Fixed/predefined-time synchronization of memristive neural networks based on state variable index coefficient. *Neurocomputing* **2023**, *560*, 126849. [[CrossRef](#)]
47. Wang, D.; Li, L. Fixed-time synchronization of delayed memristive neural networks with impulsive effects via novel fixed-time stability theorem. *Neural Netw.* **2023**, *163*, 75–85. [[CrossRef](#)]

48. Podlubny, I. *Fractional Differential Equations*; Academic Press: New York, NY, USA, 1999.
49. Lakshmikantham, V.; Vatsala, A. Basic theory of fractional differential equations. *Nonlinear Anal.* **2008**, *69*, 2677–2682. [[CrossRef](#)]
50. Zhang, S.; Yu, Y.; Wang, H. Mittag-Leffler stability of fractional-order hopfield neural networks. *Nonlin. Anal. Hybrid Syst.* **2015**, *16*, 104–121. [[CrossRef](#)]
51. Yu, J.; Hu, C.; Jiang, H. Corrigendum to Projective synchronization for fractional neural networks. *Neural Netw.* **2015**, *67*, 152–154. [[CrossRef](#)]
52. Kong, F.; Zhu, Q.; Sakthivel, R. Finite-time and fixed-time synchronization analysis of fuzzy Cohen-Grossberg neural networks with piecewise activations and parameter uncertainties. *Eur. J. Control* **2020**, *56*, 179–190. [[CrossRef](#)]

Disclaimer/Publisher’s Note: The statements, opinions and data contained in all publications are solely those of the individual author(s) and contributor(s) and not of MDPI and/or the editor(s). MDPI and/or the editor(s) disclaim responsibility for any injury to people or property resulting from any ideas, methods, instructions or products referred to in the content.